

# Mitigating Long-tail Distribution in Oracle Bone Inscriptions: Dataset, Model, and Benchmark

Jinhao Li\*  
lomljhoax@stu.ecnu.edu.cn  
East China Normal University  
Shanghai, China

Zijian Chen\*  
zijian.chen@sjtu.edu.cn  
Shanghai Jiao Tong University  
Shanghai, China

Runze Jiang  
20040329jrz@sjtu.edu.cn  
Shanghai Jiao Tong University  
Shanghai, China

Tingzhu Chen†  
tingzhuchen@sjtu.edu.cn  
Shanghai Jiao Tong University  
Shanghai, China

Changbo Wang†  
cbwang@cs.ecnu.edu.cn  
East China Normal University  
Shanghai, China

Guangtao Zhai  
zhaiguangtao@sjtu.edu.cn  
Shanghai Jiao Tong University  
Shanghai, China

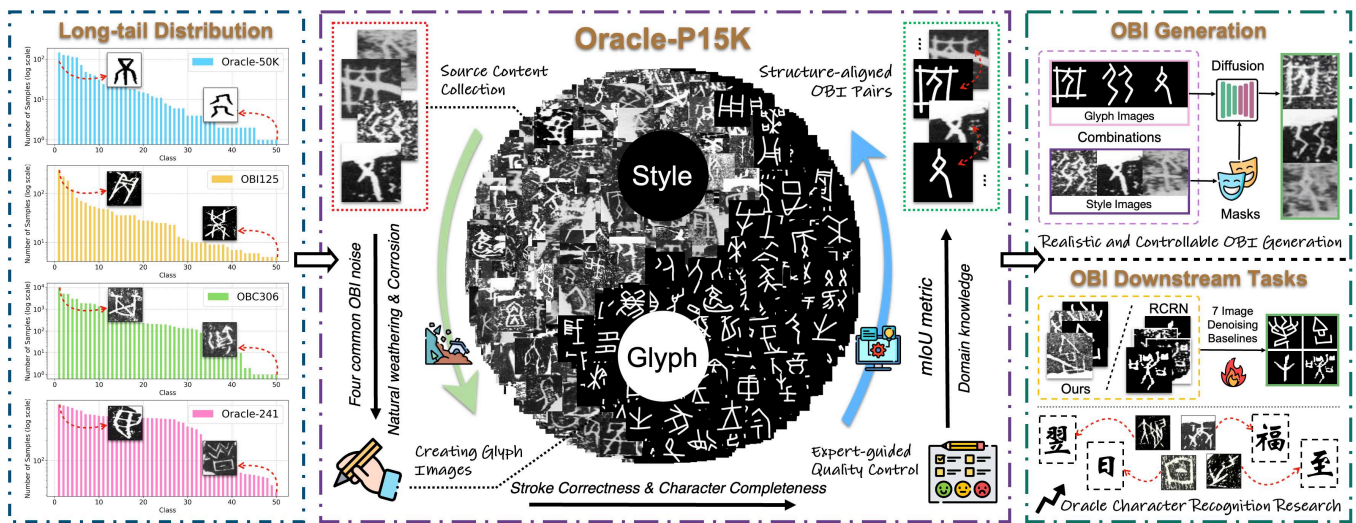


**Figure 1: Overview of the proposed Oracle-P15K dataset.** The dataset comprises 14,542 OBI images with structure-aligned expert-annotated glyphs. Based on this, we present a pseudo OBI image generator, namely OBIDiff, to alleviate the long-tail distribution problem in current OBI datasets. Extensive experiments demonstrate both the necessity of Oracle-P15K and the effectiveness of OBIDiff in improving the performance of downstream OBI tasks.

## Abstract

The oracle bone inscription (OBI) recognition plays a significant role in understanding the history and culture of ancient China. However, the existing OBI datasets suffer from a long-tail distribution problem, leading to biased performance of OBI recognition models across majority and minority classes. With recent advancements in generative models, OBI synthesis-based data augmentation has become a promising avenue to expand the sample size of minority classes. Unfortunately, current OBI datasets lack large-scale structure-aligned image pairs for generative model training. To address these problems, we first present the Oracle-P15K, a structure-aligned OBI dataset for OBI generation and denoising, consisting of 14,542 images infused with domain knowledge from OBI experts. Second, we propose a diffusion model-based pseudo OBI generator, called OBIDiff, to achieve realistic and controllable OBI generation. Given a clean glyph image and a target rubbing-style image, it

can effectively transfer the noise style of the original rubbing to the glyph image. Extensive experiments on OBI downstream tasks and user preference studies show the effectiveness of the proposed Oracle-P15K dataset and demonstrate that OBIDiff can accurately preserve inherent glyph structures while transferring authentic rubbing styles effectively.

## CCS Concepts

• **Computing methodologies** → *Computer vision tasks.*

## Keywords

Oracle Bone Inscriptions, Diffusion Model, Dataset, Image Denoising, Oracle Character Recognition

## 1 Introduction

Oracle bone inscriptions (OBI), dating from the late Shang Dynasty (1400–1100 B.C.), are the earliest evidence of Chinese writing. They

\*Both authors contributed equally to this research.

† Corresponding Authors.

document divination practices and prayers to deities, offering valuable insights into the language, society, and beliefs of ancient China. The discovery and study of OBI provide a unique perspective on early Chinese civilization. With the advancements of artificial intelligence, various models have been proposed for different OBI information processing tasks, such as OBI recognition [36], denoising [32, 33], deciphering [1, 7, 11, 20, 25, 34], etc. The OBI datasets are essential for these deep learning-based methods. However, most existing OBI datasets suffer from a long-tail distribution problem. As shown in Fig. 1, the largest class in the OBC306 [19] contains 51,796 samples, while the smallest class only contains 2 samples. Consequently, OBI-related models achieve superior performance in majority classes while underperforming in minority classes.

To overcome this issue, three strategies have been proposed for the long-tail distribution problem in OBI datasets: few/zero-shot learning, imbalanced learning, and cross-modal learning [23]. Few/zero-shot learning and imbalanced learning [4, 5, 13, 49] tackle the challenge of data scarcity with network improvement and data augmentation. However, network improvement is constrained by writing variability and severe noise in OBI. Cross-modal learning [36, 37] mitigates writing variability by leveraging both scanned and handprint data but still struggles to handle noisy images and address more complex scenarios. Therefore, various researchers use data augmentation [2, 3, 18, 24, 26, 39] to expand the training set with the most powerful generative models, i.e., generative adversarial networks [9, 51] and diffusion models [15, 31, 46]. For example, AGTGAN [18] proposed an unsupervised generative adversarial network to generate characters with diverse glyphs and realistic textures, thereby supplementing the dataset with scanned OBI images. ADA [24] introduced an end-to-end generative adversarial framework that produces synthetic data through convex combinations of all available samples in tail classes. However, these methods suffer from low quality and a lack of controllability, which limits their applications in fine-grained OBI recognition tasks.

In this paper, we aim to develop a method to generate realistic and controllable OBI images by incorporating glyphs and styles. The glyphs indicate the semantics of the OBI and the styles describe the unique texture caused by thousands of years of natural weathering and corrosion. However, training such a model requires large-scale structure-aligned glyph and style image pairs. To the best of our knowledge, none of the existing OBI datasets can provide such labor-intensive and expertise-demanding pairs. The Oracle-241 [36] dataset contains OBI image pairs, which are only class-aligned. Shi *et al.* [33] proposes a structure-aligned dataset for OBI denoising, i.e., RCRN, which is limited in scale and quality. Therefore, we construct Oracle-P15K, a large-scale structure-aligned OBI dataset comprising 14,542 images infused with domain knowledge from OBI experts. The Oracle-P15K dataset can also serve as a comprehensive benchmark for researchers to develop and evaluate their methods for dealing with other OBI information processing tasks, such as OBI denoising, recognition, etc.

Based on our Oracle-P15K, we propose a novel diffusion model for realistic and controllable OBI generation, namely OBIDiff. It can transfer the style of the glyph image into that of the style image. Our model consists of a frozen autoencoder, a pre-trained stable diffusion (SD) model, a trainable glyph encoder, and a trainable style encoder. Unlike natural image styles, OBI image styles are too

complicated to define by a few text prompts. Therefore, the style encoder integrates a CLIP [30] image encoder and a linear layer to align the image and text embeddings in the latent space. In the training process, the glyph and style encoders extract glyph and style conditions to guide the SD model in generating the target image. It is worth noting that the characters in the glyph and style images should be the same. As a result, the glyph of the style image hampers the training of the glyph encoder. To tackle this problem, we leverage the structure-aligned glyph image to mask the glyph of the style image. In the inference process, the characters in the glyph and style images are different so that we can transfer the style of the glyph image into that of the style image. In conclusion, our key contributions can be summarized as follows:

- **Introduction of Oracle-P15K:** We construct Oracle-P15K, the first OBI dataset containing structure-aligned image pairs, specifically for pseudo OBI generation. This dataset consists of 14,542 images across 239 classes that cover four commonly existing types of noise in OBI.
- **Controllable Pseudo OBI Generator:** We present a dedicated diffusion model, namely OBIDiff, to address the huge sample size discrepancies in current OBI datasets for mitigating the long-tail distribution problem that hinders downstream OBI tasks. By controllably combining learned OBI noise representations into glyph generation, OBIDiff achieves realistic and expert-confused OBI generation.
- **Comprehensive Downstream Task Evaluation:** We demonstrate the contribution of Oracle-P15K to improving the performance of downstream OBI tasks. Specifically, it enhances the capability of OBI denoising methods to restore severely distorted oracle bone characters.

## 2 Related Work

### 2.1 Oracle Bone Inscription Datasets

In the past decade, various oracle bone inscription (OBI) datasets have been established for different OBI information processing tasks. The existing OBI datasets can be categorized into rubbings and handprints from the perspective of content sources. For instance, the OBC306 [19], OBI125 [41], Oracle-MNIST [35] and O2BR [1] are rubbing datasets for OBI recognition, whose images are collected from oracle bone publications or shot from real OBI materials. In contrast, the Oracle-20K [12], Oracle-50K [13], and HWOBC [22] are handprint datasets for OBI recognition, whose images are imitatively written by experts. Meanwhile, the Oracle-241 [36] is another OBI recognition dataset containing handprints and rubbings. Besides, the OracleBone8000 [44], OB-Rejoin [43], and OBI-rejoin [1] are built for OBI rejoining. Moreover, the EVOBC [10] and HUST-OBC [38] are proposed to understand the evolution of OBI. With the advent of diffusion models and large multimodal models (LMs), they show great potential for OBI deciphering. However, these datasets cannot provide large-scale structure-aligned image pairs, which hinders the development of OBI generation and denoising. A detailed comparison of these datasets is provided in Table 1.

### 2.2 Oracle Bone Inscription Generation

Traditional oracle bone inscription generation methods augment samples through transformations, such as random rotations and

**Table 1: Summary of the existing oracle bone inscription datasets. The Min, Max, and SD denote the minimum, maximum, and standard deviation of sample counts per class in the dataset, respectively. Specifically, we report the distribution information of the test set of our Oracle-P15K separately. The alignment indicates whether the dataset is structure-aligned or not.**

| Type     | Dataset             | Year | #Classes | #Images | Resolution | Min   | Max    | SD      | Availability | Alignment |
|----------|---------------------|------|----------|---------|------------|-------|--------|---------|--------------|-----------|
| Unpaired | Oracle-20K [12]     | 2016 | 261      | 20,039  | 50×50      | -     | -      | -       | ✗            | ✗         |
|          | Oracle-50K [13]     | 2020 | 2,668    | 59,081  | 50×50      | 1     | 388    | 39.1    | ✓            | ✗         |
|          | HWOBC [22]          | 2020 | 3,881    | 83,245  | 400×400    | 19    | 24     | 1.2     | ✓            | ✗         |
|          | OBC306 [19]         | 2019 | 306      | 309,551 | <382×478   | 1     | 25,898 | 2,428.3 | ✓            | ✗         |
|          | OracleBone8000 [44] | 2020 | -        | 129,770 | -          | -     | -      | -       | ✗            | ✗         |
|          | OBI25 [41]          | 2022 | 125      | 4,257   | <278×473   | 5     | 307    | 42.3    | ✓            | ✗         |
|          | OB-Rejoin [43]      | 2022 | -        | 998     | <1408×1049 | -     | -      | -       | ✗            | ✗         |
|          | Oracle-MNIST [35]   | 2023 | 10       | 30,222  | 28×28      | 2,628 | 3,699  | 351.1   | ✓            | ✗         |
|          | EVOBC [10]          | 2024 | 13,714   | 229,170 | <465×857   | 0     | 1,000  | 48.0    | ✓            | ✗         |
|          | HUST-OBC [38]       | 2024 | 10,999   | 140,053 | <400×520   | 1     | 307    | 39.6    | ✓            | ✗         |
| Paired   | O2BR [1]            | 2025 | -        | 800     | <2664×2167 | -     | -      | -       | ✓            | ✗         |
|          | OBI-rejoin [1]      | 2025 | -        | 200     | <2913×1268 | -     | -      | -       | ✓            | ✗         |
|          | Oracle-241 [36]     | 2022 | 241      | 78,565  | <588×700   | 29    | 687    | 175.6   | ✓            | ✗         |
| Paired   | RCRN [33]           | 2022 | -        | 3,212   | <520×668   | -     | -      | -       | ✓            | ✓         |
|          | Oracle-P15K         | 2025 | 239      | 14,542  | 128×128    | 60/22 | 60/114 | 0/23.8  | ✓            | ✓         |

flipping. Recently, RPC [3] generates additional images by mimicking noise, i.e., dense white regions, with various polygons. In addition, MA [26] leverages feature information from both majority and minority classes to augment samples in minority classes, thereby achieving better recognition performance than traditional methods. Moreover, Orc-Bert [13] and FFD [49] focus on the few-shot learning of handprint data and augment the few-shot classes by learning and transforming the stroke vectors of OBI, which may be hampered by the severe noise in rubbing data. More recently, CDA [39], AGTGAN [18], ADA [24], STSN [36], and UDCN [37] consider OBI generation an image translation problem and leverage generative adversarial networks to swap texture features across domains. However, they suffer from a lack of controllability and training instability. In contrast, our OBI-Diff can generate realistic OBI images while being controllable.

### 2.3 Downstream Oracle Bone Inscription Tasks

Downstream oracle bone inscription tasks include challenges in six domains: rejoining, classification, retrieval, deciphering, denoising, and recognition [1]. Among them, OBI rejoining [43, 44] restores the original appearance of oracle bones and offers complete and accurate information for OBI researchers. In addition, OBI retrieval [6, 17, 21, 27] collects similar OBI samples from existing datasets, thereby facilitating more large-scale database construction. Moreover, OBI classification helps distinguish real rubbings from distortions, which is a practical requirement for human experts. Most recently, various OBI deciphering models [1, 7, 11, 20, 25, 34] have also been proposed to understand these ancient Chinese characters by leveraging diffusion models and LMMs. Overall, all these tasks rely on OBI recognition [29, 36, 50], which suffers from the long-tail distribution problem in current OBI datasets. Recent advancements in generative models offer promising avenues for addressing this issue through data augmentation. However, training such models typically requires structure-aligned image pairs.

Similarly, OBI denoising [21, 32, 33] also relies on such pairs to effectively remove noise while preserving glyph structures. Hence, building a structure-aligned dataset for both OBI generation and denoising is an urgent need in the OBI research community.

## 3 The Oracle-P15K Dataset

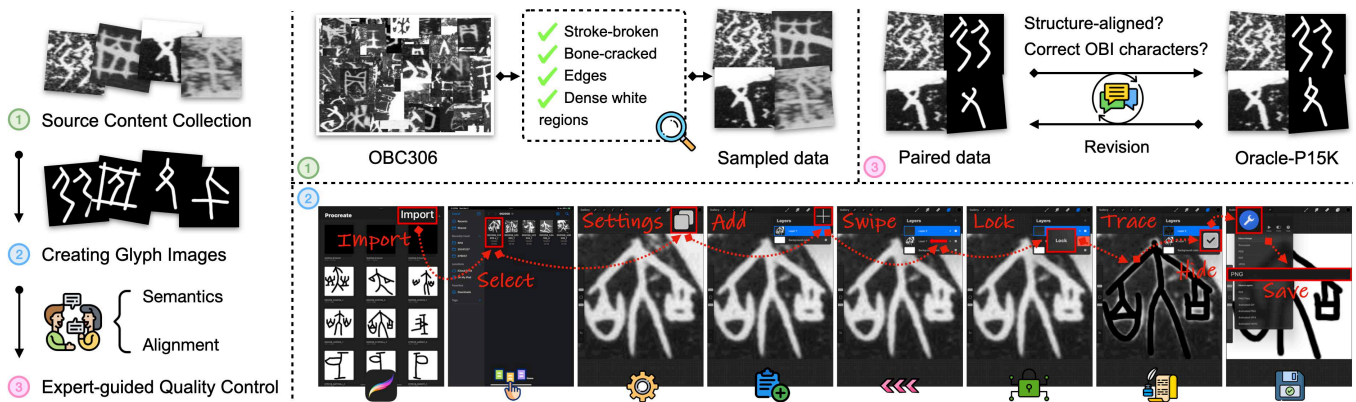
### 3.1 Construction Pipeline

Fig. 2 shows the overall construction pipeline of our Oracle-P15K. The following explains how we build the dataset in detail.

**Source Content Collection:** We collect style images from the OBC306 [19], a large-scale OBI dataset specifically constructed for OBI recognition. According to OBC306, the noise of OBI can be categorized into stroke-broken, bone-cracked, edges, and dense white regions. Thus, we meticulously select representative OBI images from the OBC306 to ensure the coverage of the four noise types in OBI. Specifically, we select 30 images for each of the 200 head classes in OBC306. In addition, all samples of the 39 tail classes are collected for testing to avoid overlapping. Therefore, the whole dataset contains 7,271 image pairs across 239 classes.

**Creating glyph images:** After collecting style images, we use an iPad Pro, an Apple Pencil, and the Procreate software to create the corresponding structure-aligned glyph images. All the glyph images are written using a 7-pixel calligraphy monoline-style brush in Procreate. We provide the operational details in Appendix B. Specifically, there are two categories of special cases we may encounter in the writing procedure:

- **Stroke-broken:** Some strokes of OBI are broken due to thousands of years of natural weathering and corrosion. In this case, we reconstruct the characters by completing the broken strokes.



**Figure 2: Construction pipeline of our Oracle-P15K. Step-1: We focus on four types of noise in OBI rubbings and take them as targets for source content sampling. Step-2: OBI experts are invited to create glyph images manually. Step-3: We conduct a post-quality examination to ensure the reliability and alignment of OBI image pairs.**

- **Bone-cracked & Edges:** Some strokes of OBI are incomplete or covered by noisy regions caused by long burial and careless excavation. In this case, we complete the glyphs with domain knowledge from the annotator.

It should be noted that the glyph image features black strokes on a white background, which is an inverse color configuration compared to the style image. Therefore, we invert the color configuration of the glyph images after construction.

**Expert-guided Quality Control:** We design a quality examination procedure to ensure the quality of the structure-aligned OBI image pairs. Firstly, we conduct a human evaluation involving two OBI experts to assess whether the handprint characters represent correct OBI characters. Moreover, the characters in the glyph images should be structure-aligned with those in the corresponding style images. The experts record the glyph images that fail to meet the quality standards. Any glyph image recorded by one of the experts is discarded. Finally, the annotator is required to revise all discarded images until they faithfully represent the correct OBI characters and achieve satisfied structure alignment.

Considering the limitation of human evaluation in assessing the structure alignment between glyph and style images, we develop an automatic evaluation program to measure the IoU of glyphs between glyph and style images. Any glyph image is discarded if the IoU between it and its corresponding style image is below 0.8. Finally, our Oracle-P15K achieves an mIoU of 0.865.

### 3.2 Dataset Statistics

As shown in Table 1, we compare the proposed Oracle-P15K with other OBI datasets. It can be observed that: (1) Most datasets have reached a 10,000 scale, providing support for the research of machine learning. (2) Unlike other datasets, which only contain handprints, rubbings, or class-aligned image pairs, our Oracle-P15K consists of structure-aligned image pairs infused with domain knowledge from OBI experts. (3) Our dataset is a distribution-balanced dataset, which prevents bias in model training and evaluation. Specifically, it achieves 60, 60, and 0 in terms of minimum, maximum, and standard deviation of sample counts per class in the

training and validation sets, respectively. In summary, while the Oracle-P15K and other OBI datasets are all large-scale, our dataset focuses on structure-aligned OBI image pairs, thereby facilitating the development of robust OBI generation and denoising models.

Empirically, we randomly split the samples selected from the 200 head classes of the OBC306 dataset into two subsets for training and validation in an 8:2 ratio. The test set is collected from the 39 tail classes of the OBC306 dataset and does not overlap with the images in the training and validation sets.

### 3.3 Application Scenarios

The Oracle-P15K dataset can contribute to various OBI information processing tasks including, but not limited to, OBI generation and denoising. By enhancing the quality and diversity of OBI images, it improves the robustness and accuracy of OBI recognition models. Specifically, our Oracle-P15K benefits the OBI research community in three folds:

- **Catering OBI Researchers Better:** Existing OBI datasets often contain misannotated images, which can hinder research accuracy. To provide OBI researchers with more fine-grained and reliable data, our Oracle-P15K dataset has undergone multiple rounds of validation by OBI experts.
- **Facilitating OBI Generation Models:** Our dataset enables OBI generation models to generate realistic and controllable OBI images, thereby improving the recognition accuracy of the tail class significantly.
- **More Comprehensive and Practical OBI Denoising Benchmark:** Our dataset contains 7,271 real-world OBI image pairs across 4 types of noise. Compared to the previous OBI denoising benchmark, i.e., RCRN, it is more comprehensive and closer to the real-world OBI denoising scenario.

## 4 Pseudo OBI Generator

Inspired by ControlNet [46], we propose to generate pseudo OBI images by incorporating glyphs and styles. As shown in Fig. 4, our OBIDiff consists of an autoencoder, a stable diffusion (SD) [31] model, a glyph encoder, and a style encoder. Firstly, we feed OBIDiff

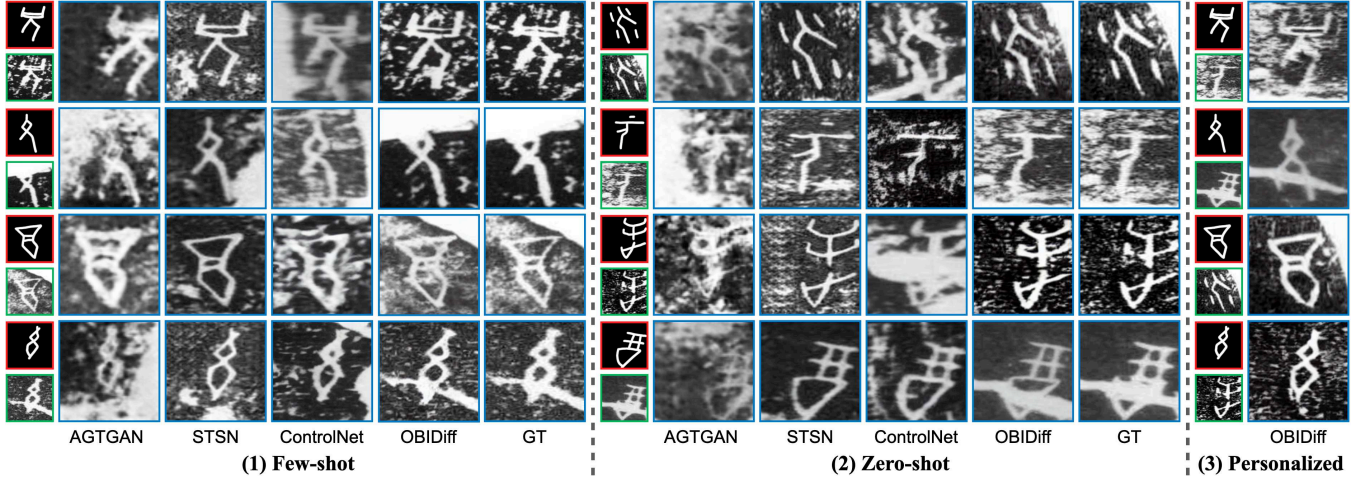


Figure 3: Comparison of the OBI generation results on the Oracle-P15K dataset. The red, green, and blue boxes denote the glyph, style, and generated images, respectively. Three evaluation settings are considered. (1) Few-shot: the characters in the training and validation sets are the same. (2) Zero-shot: the characters in the training and test sets are not overlapped. (3) Personalized: the glyph and style images are not aligned.

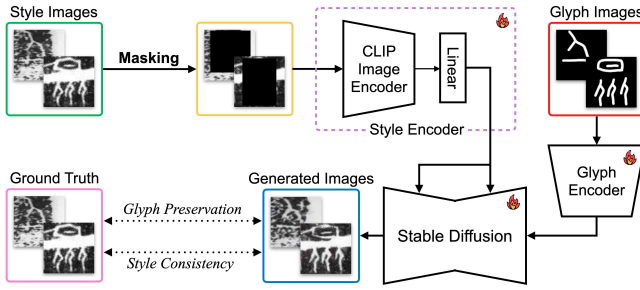


Figure 4: Architecture of our OBIDiff.

with an input image  $x_0$ , a glyph image  $x_g$ , and a style image  $x_s$ . Then, the autoencoder extracts features from  $x_0$  to put the diffusion process into latent space. Subsequently, the glyph conditions  $\tau_g$  are extracted by the glyph encoder  $\mathcal{E}_g$  to concatenate with initial noise for glyph guidance:

$$\tau_g = \mathcal{E}_g(x_g). \quad (1)$$

In addition to glyph conditions, style conditions play a crucial role in controlling the intricate visual characteristics of the generated images. However, it is difficult to describe the complex styles of OBI images in natural languages. Therefore, we introduce the style encoder  $\mathcal{E}_s$  to learn the specific style representations from the real-world OBI rubbing images. The style encoder  $\mathcal{E}_s$  comprises a CLIP image encoder  $\mathcal{E}_c$  and a linear layer  $l$ . The CLIP image encoder  $\mathcal{E}_c$  extracts image embeddings and the linear layer  $l$  aligns them with text embeddings in the latent space:

$$\tau_s = l(\mathcal{E}_c(x_s)). \quad (2)$$

Finally, the SD model, glyph encoder, and style encoder are optimized jointly by the simple loss of latent diffusion models [31] computed on the latent noise of the forward process and the reverse

process:

$$\mathcal{L} = \mathbb{E}_{x_0, t, \tau_g, \tau_s, \epsilon \sim \mathcal{N}(0,1)} [\| \epsilon - \epsilon_\theta(x_t, t, \tau_g, \tau_s) \|_2^2], \quad (3)$$

where  $\mathcal{L}$  is the overall learning objective of our OBIDiff.  $x_t$  denotes a noisy image produced in time  $t$ .  $\epsilon_t$  represents the learning network, which predicts the noise added to the noisy image  $x_t$ . Notably, the style image  $x_s$  is obtained from the input image  $x_0$ , which is structure-aligned with the glyph image  $x_g$ . In the inference process, the style image is obtained from other images. In this case, the style embeddings of the style image guide the generative model in generating a new style OBI image.

However, the glyph encoder fails to learn the glyph conditions in the training process. Consequently, the generated images are identical to the style images in the inference process, which results from the glyph interference in the training process. To address this issue, we mask the glyph of the style image with a bounding box computed by detecting the white pixels in the structure-aligned glyph image. This strategy alleviates the influence of the glyph while preserving the main information of the style image, which effectively enhances the capability of the model to learn the glyph and style conditions.

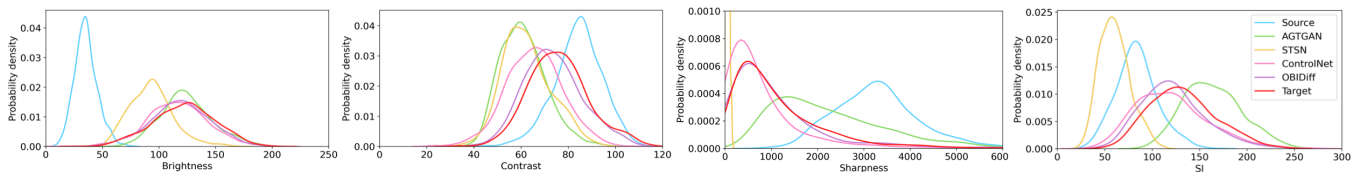
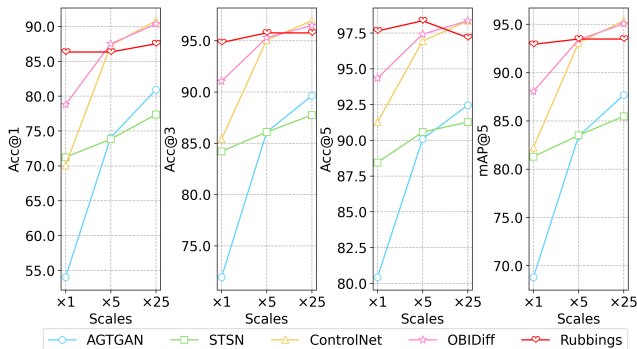
## 5 Experiments

### 5.1 Experimental Settings

**Datasets.** Our OBIDiff is evaluated on the validation and testing sets of the proposed Oracle-P15K dataset. Three generation strategies are considered. First, the characters of the training and validation sets are the same. Second, a zero-shot generation case is formed by performing inference on 39 tail classes from the testing set. Third, we introduce personalized OBI generation by substituting the style images with different characters. Besides, we collect the other 424 images across 39 tail classes from the test set of the OBC306 to evaluate the models on the OBI recognition task.

**Table 2: Quantitative comparisons of OBI generation results on the Oracle-P15K dataset. The improvements of our OBIDiff against other baselines are delimited by slashes. The best and second-best results are in red and blue, respectively.**

| Methods         | Few-shot              |                       |                       |                       |                       |                    | Zero-shot          |                    |                    |
|-----------------|-----------------------|-----------------------|-----------------------|-----------------------|-----------------------|--------------------|--------------------|--------------------|--------------------|
|                 | L1 Loss↓              | RMSE↓                 | PSNR↑                 | SSIM↑                 | LPIPS↓                | FID↓               | Acc@1↑             | Acc@3↑             | Acc@5↑             |
| Rubbings (ref)  | -                     | -                     | -                     | -                     | -                     | -                  | 86.32              | 94.81              | 97.64              |
| Handprints      | 0.3874/0.2682         | 0.4895/0.2881         | 6.2084/7.7200         | 0.1211/0.3628         | 0.5440/0.3591         | 344.1/271.3        | 14.99/61.74        | 28.19/60.85        | 36.69/56.82        |
| AGTGAN [18]     | 0.3184/0.1992         | 0.3981/0.1967         | 8.0039/5.9245         | 0.0778/0.4061         | 0.5012/0.3163         | 196.0/123.2        | 54.01/24.76        | 71.93/19.11        | 80.42/13.92        |
| STSN [36]       | <b>0.2648</b> /0.1456 | <b>0.3581</b> /0.1567 | <b>8.9290</b> /4.9994 | <b>0.2486</b> /0.2353 | <b>0.3662</b> /0.1813 | 110.3/37.5         | <b>71.23</b> /7.54 | 84.20/6.84         | 88.44/5.90         |
| ControlNet [46] | 0.2877/0.1685         | 0.3743/0.1729         | 8.5403/5.3881         | 0.1776/0.3063         | 0.4147/0.2298         | <b>100.0</b> /27.2 | 70.05/8.72         | <b>85.38</b> /5.66 | <b>91.27</b> /3.07 |
| OBIDiff         | <b>0.1192</b>         | <b>0.2014</b>         | <b>13.9284</b>        | <b>0.4839</b>         | <b>0.1849</b>         | <b>72.8</b>        | <b>78.77</b>       | <b>91.04</b>       | <b>94.34</b>       |

**Figure 5: Feature distribution comparisons among generated images from baseline methods and our OBIDiff.****Figure 6: Recognition accuracy of augmented rare OBI images w.r.t. style image at different scales.**

To the best of our knowledge, RCRN [33] is the only existing dataset consisting of structure-aligned OBI image pairs. Therefore, we also conduct parallel experiments on RCRN to demonstrate the superiority of our Oracle-P15K on the OBI denoising task. We collect 4,499 images across 200 head classes from the OBC306 dataset to evaluate their denoising performance. Note that these images and the proposed Oracle-P15K dataset do not overlap.

**Baseline Methods.** For the OBI generation task, we compare our OBIDiff with ControlNet [46] and two OBI-specialized image generation models, AGTGAN [18] and STSN [36]. For the OBI denoising task, we benchmark six representative generic image denoising models (DnCNN [45], InvDN [28], Uformer [40], Restormer [42], KBNNet [48], and CGNet [8]) as well as an OBI denoising method, CharFormer [32]. All baselines are retained on OBI task-related datasets using official implementations with default configurations.

**Evaluation Metrics.** We apply six common metrics in image generation tasks, including L1 Loss, RMSE, PSNR, SSIM [16], LPIPS [47], FID [14]. Since the significant stroke disparity between the handprints and rubbings in our Oracle-P15K, it is irrational to evaluate the OBI denoising performance by standard low-level vision metrics, such as PSNR and SSIM [16]. Therefore, an efficient OBI classifier based on ResNet-50 is built to evaluate their performance in tasks oriented to oracle character recognition. More implementation details are in Appendix C.

## 5.2 Main Results

**OBI generation.** Fig. 3 presents the qualitative comparisons between our OBIDiff and other OBI generation methods. We observe that our OBIDiff accurately preserves glyph structures while transferring complex styles effectively. In contrast, other methods struggle to maintain the intrinsic glyphs or reproduce the styles properly. This is primarily because other methods lack effective style controllability. For example, our OBIDiff shows robust generation ability across four different noise types. However, STSN produces duplicated patterns in the third zero-shot case. Moreover, even in the few-shot scenarios, AGTGAN and ControlNet generate artifacted noise in the second and third cases, respectively. More generated results from our OBIDiff can be found in the Appendix.

Additionally, we report the quantitative comparisons between our OBIDiff and other OBI generation methods in Table 2. The improvements of our OBIDiff against other OBI generation methods are delimited by slashes. We compare three groups of images: handprint (glyph) images, rubbing (style) images, and generated images. For each glyph image, we generate the augmented image using the corresponding style image. It can be observed that our OBIDiff outperforms other OBI generation methods across all six low-level metrics by a large margin. This can be attributed to the glyph and style encoders, which inject glyph and style information

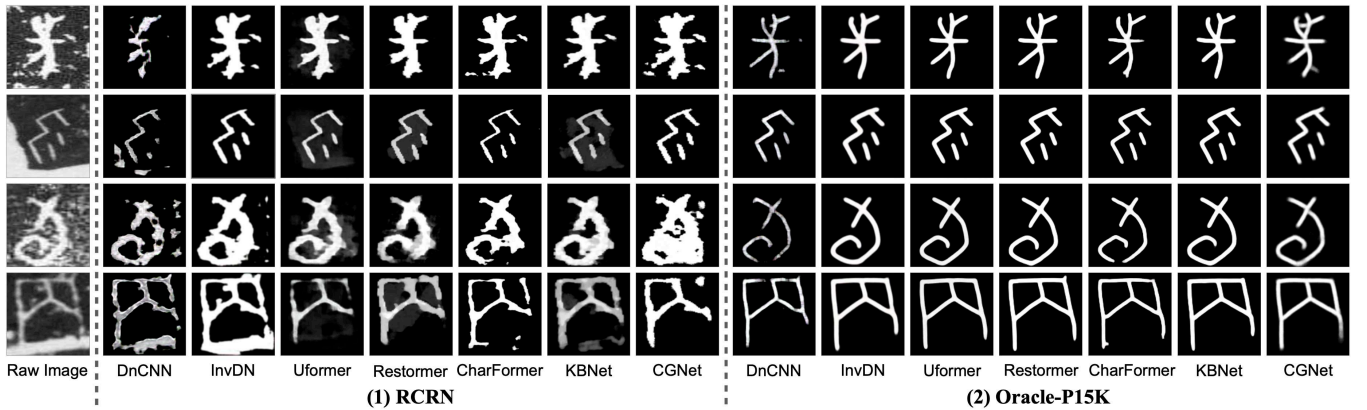


Figure 7: Performance comparison of OBI denoising methods on the RCRN and Oracle-P15K datasets.

Table 3: Quantitative comparisons (oracle character recognition accuracy) of OBI denoising methods trained on the RCRN/Oracle-P15K datasets. We also report the improvements of the models trained on our Oracle-P15K against the original rubbings.

| Metrics | Rubbings | DnCNN [45]                   | InvDN [28]                   | Uformer [40]                 | Restormer [42]               | CharFormer [32]              | KBNet [48]                   | CGNet [8]                    |
|---------|----------|------------------------------|------------------------------|------------------------------|------------------------------|------------------------------|------------------------------|------------------------------|
| Acc@1↑  | 85.97    | 62.06/85.83 <sub>-0.14</sub> | 77.28/89.62 <sub>+3.65</sub> | 84.71/89.83 <sub>+3.86</sub> | 81.42/89.90 <sub>+3.93</sub> | 78.19/88.43 <sub>+2.46</sub> | 83.17/90.25 <sub>+4.28</sub> | 74.05/90.67 <sub>+4.70</sub> |
| Acc@3↑  | 95.30    | 76.37/94.18 <sub>-1.12</sub> | 88.43/96.70 <sub>+1.40</sub> | 94.46/96.56 <sub>+1.26</sub> | 92.43/96.84 <sub>+1.54</sub> | 89.41/96.21 <sub>+0.91</sub> | 93.34/97.05 <sub>+1.75</sub> | 86.75/97.62 <sub>+2.32</sub> |
| Acc@5↑  | 97.12    | 81.77/96.56 <sub>-0.56</sub> | 91.73/98.04 <sub>+0.92</sub> | 96.56/98.11 <sub>+0.99</sub> | 95.30/98.25 <sub>+1.13</sub> | 92.43/97.90 <sub>+0.78</sub> | 95.72/98.11 <sub>+0.99</sub> | 89.90/98.53 <sub>+1.41</sub> |

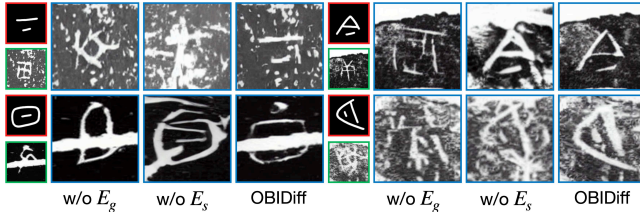


Figure 8: The ablation study of glyph and style encoders.

into the SD model to generate realistic and controllable OBI images. Moreover, our OBIDiff achieves state-of-the-art performance in the OBI recognition task. On the one hand, the low recognition accuracy of handprints underscores the significant disparity between handprints and rubbings. We also provide visualization studies in Appendix D to support this conclusion. On the other hand, while ControlNet shows promising results on Acc@3 (85.38%) and Acc@5 (91.27%), it performs poorly in terms of Acc@1 (70.05%). In comparison, our OBIDiff can improve Acc@1 by 8.72% and 7.54% against ControlNet and STSN, respectively. These results demonstrate the substantial impact of our OBIDiff in enhancing the recognition accuracy for zero-shot classes. Furthermore, we calculate four low-level features including brightness, contrast, sharpness, and spatial information (SI), thereby providing a large visual space in which to plot and analyze content diversities of the generated images from different models. Fig. 5 shows the fitted kernel distribution of each selected feature. Compared to other images, the images generated by our OBIDiff exhibit a more similar probability density. It indicates that our OBIDiff generates more visually pleasant results.

Besides, we investigate the impact of data augmentation by adjusting the scales of data augmentation. Fig. 6 presents the recognition accuracy of augmented images generated by the proposed OBIDiff and other OBI generation methods w.r.t. the scale of data augmentation. All models show consistent progress as the scale of data augmentation increases, except for the original rubbings, which experience a notable decline in Acc@5 at  $\times 25$  scale. That may be due to overfitting caused by the duplicated images. Moreover, we also find that ControlNet and our OBIDiff exhibit remarkable improvements as the scale of data augmentation increases. Compared to ControlNet, our OBIDiff achieves superior performance at  $\times 1$  scale, narrowing the gap between ControlNet and the original rubbings by half. Trained on our Oracle-P15K, ControlNet surpasses original rubbings by 1.18% in terms of Acc@3 and Acc@5 at  $\times 25$  scale, underscoring the superior quality of the proposed Oracle-P15K. Similarly, our OBIDiff yields a favorable gain of 0.71% and 1.18% over the original rubbings, which demonstrates the high quality and diversity of the generated images from our OBIDiff. Overall, our OBIDiff achieves state-of-the-art performance in mAP@5, outperforming the original rubbings by 1.58% at  $\times 25$  scale.

**OBI denoising.** Fig. 7 shows qualitative results of generic and OBI denoising models on RCRN and Oracle-P15K datasets. We report their denoising performance on four different noise types. It can be observed that the models trained on Oracle-P15K can robustly handle diverse noise types, whereas the models trained on RCRN struggle to preserve inherent glyph structures properly. For instance, DnCNN and InvDN fail to effectively restore the dense white regions and bone-cracked. Moreover, other methods remove the noise aggressively, leading to glyph damage in the fourth case of Fig. 7. Overall, it is demonstrated that the proposed

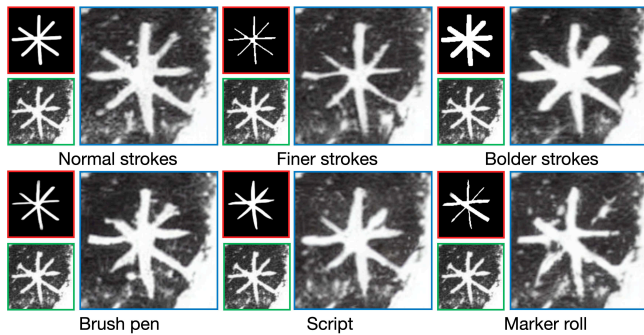


Figure 9: The ablation study of different glyph variations.

Oracle-P15K dataset can support real-world OBI denoising with large-scale structure-aligned image pairs. More denoising results from different baselines can be found in the Appendix.

In addition, we evaluate the quantitative performance of these methods. As shown in Table 5, CGNet achieves the best recognition accuracy (90.67%, 97.62%, and 98.53% in terms of Acc@1, Acc@3, and Acc@5, respectively) on Oracle-P15K and Uformer achieves the best recognition accuracy (84.71%, 94.46%, and 96.56% in terms of Acc@1, Acc@3, and Acc@5, respectively) on RCRN. It is an interesting finding that the recognition accuracy of images denoised by the models trained on RCRN is lower than that of the original rubbings. That is due to the significant disparity in image styles between RCRN and the real-world OBI rubbing images. Moreover, we can also find that DnCNN trained on Oracle-P15K achieves poor performance on the OBI recognition task while the other methods enhance the recognition accuracy. Notably, CGNet yields 4.70%, 2.32%, and 1.41% improvements against the original rubbings in terms of Acc@1, Acc@3, and Acc@5, respectively. It highlights the superior quality of our Oracle-P15K and the importance of OBI denoising in OBI recognition.

### 5.3 Ablation Studies

**Validation of glyph guidance and style guidance:** We study the function of glyph guidance and style guidance by freezing the parameters of the glyph encoder  $\mathcal{E}_g$  and the style encoder  $\mathcal{E}_s$  in the training process, respectively. The ablation results are reported in Fig. 8. It can be observed that the model generates meaningless glyph structures without the optimization of the glyph encoder. Also, the styles of generated results are uncontrollable if we freeze the parameters of the style encoder. In contrast, our OBIDiff preserves inherent glyphs while transferring the given styles effectively. Overall, our glyph and style encoders contribute to significant gains in quality and controllability.

In addition, we also explore the impact of different variations in glyph images. Specifically, we incorporate glyph images with different stroke thicknesses and writing styles in the inference process. As shown in Fig. 9, our OBIDiff generates images robustly across diverse glyph image variations, thereby ensuring its applicability to the existing handprint OBI datasets.

**Impact of masking mechanism:** The masking mechanism is designed to mitigate the influence of the glyphs in the style images.

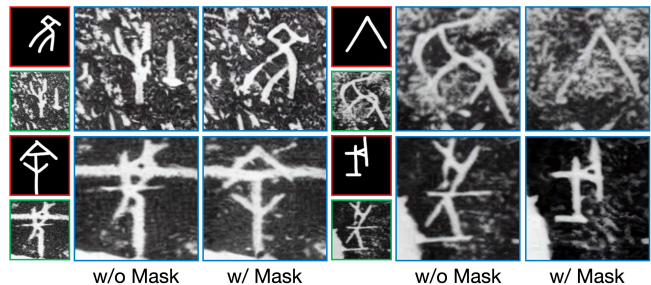


Figure 10: The ablation study of our masking mechanism.

Table 4: Results of user preference study about comparing the real rubbings and the images generated by OBIDiff.

|                   | Precision $\uparrow$ | Recall $\uparrow$ | F1 score $\uparrow$ |
|-------------------|----------------------|-------------------|---------------------|
| Human Performance | 0.52                 | 0.57              | 0.53                |

We perform an ablation study for the masking mechanism by directly feeding style images to the style encoder. The results are presented in Fig. 10. We observe that, without the masking mechanism, the generated images fail to follow the glyph conditions in the inference process. One possible reason is that the glyphs of the style images hamper the optimization of the glyph encoder in the training process. As a result, the model generates the images by simply copying the style images. Nevertheless, when the model is trained with the masking mechanism, it effectively learns the glyph and style conditions in the training process. Therefore, though the glyphs of the glyph and style images are different in the inference process, it succeeds in transferring the styles while preserving the inherent glyphs robustly.

### 5.4 User Preference Study

We conduct a user preference study to further evaluate the quality of pseudo OBI images generated by our OBIDiff. The study involves 15 college students, most majoring in Chinese language and literature. To facilitate the evaluation process, we develop a web-based user interface with automated navigation. In each round, the interface displays either a ground truth image or a pseudo image generated by our OBIDiff. Participants are asked to determine whether the current image is a real-world OBI rubbing image or a generated image. After completing 100 rounds, they will receive a brief report summarizing their evaluation results. We show the average precision, recall, and F1 score from the user preference study in Table 4. It can be observed that the performance in all three metrics is marginally above 0.5 (*random guess*), demonstrating the remarkable similarity between the generated images and real-world rubbing images. The details of the user preference study are shown in Appendix E.

### 5.5 Limitations

Although our method can transfer typical styles to some glyphs, it has two main limitations. First, our model requires a handprint glyph image as one of the inputs, which involves some manual

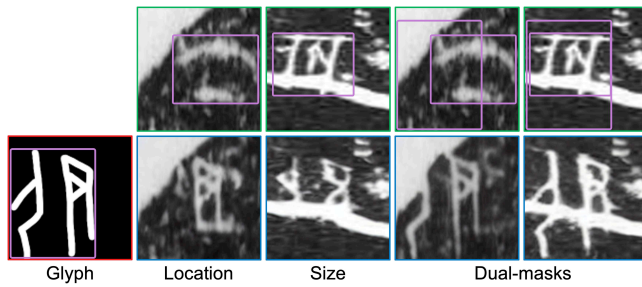


**Figure 11: Inconsistency in bounding boxes of glyph and style images. Purple boxes indicate the bounding boxes of the characters. We adopt a dual-masking mechanism to address this issue.**

effort. While various handprint OBI datasets are available, this issue still limits its applications in large-scale personalized OBI generation. Second, we introduce a masking mechanism in the style conditioning process to alleviate the influence caused by the glyphs of the style images. However, the location and size of the bounding boxes of the characters in the style images during the inference process may not always be consistent with those in the glyph images. As shown in Fig. 11, we adopt a dual-masking mechanism to address this issue. Nevertheless, the mask computed from the glyph

image may obscure critical style information in the corresponding style image, leading to a few failed cases in the inference process. Fortunately, this issue can be mitigated by manually selecting the bounding boxes-aligned style images.

## 6 Conclusion

In this paper, we introduce Oracle-P15K, a structure-aligned OBI dataset comprising unique glyph images provided by OBI experts for OBI generation and denoising models. Based on this, we propose a pseudo OBI generator to address the long-tail distribution problem in current OBI datasets, thus significantly improving the recognition accuracy of small-sample characters. Our dataset enables new research directions, such as developing more powerful generative models for rare OBI protection and addressing authenticity concerns like misinformation by identifying fake OBI. Extensive experiments and user preference studies demonstrate the effectiveness of our model on high-quality and noise-controllable OBI generation. Besides, our dataset can also serve as a comprehensive and practical OBI denoising benchmark.

## Acknowledgments

This work was supported by the National Social Science Foundation of China (24Z300404220) and the Shanghai Philosophy and Social Science Planning Project (2023BYY003).

## References

- [1] Zijian Chen, Tingzhu Chen, Wenjun Zhang, and Guangtao Zhai. 2024. OBI-Bench: Can LMMs Aid in Study of Ancient Script on Oracle Bones? *arXiv preprint arXiv:2412.01175* (2024).
- [2] Zijian Chen, Wei Sun, Haoning Wu, Zicheng Zhang, Jun Jia, Ru Huang, Xiongkuo Min, Guangtao Zhai, and Wenjun Zhang. 2024. Study of Subjective and Objective Naturalness Assessment of AI-Generated Images. *IEEE Transactions on Circuits and Systems for Video Technology* (2024).
- [3] Liu Dazheng. 2021. Random Polygon Cover for Oracle Bone Character Recognition. In *Proceedings of the 2021 5th International Conference on Computer Science and Artificial Intelligence*. 138–142.
- [4] Xiaolei Diao, Daqian Shi, Jian Li, Lida Shi, Mingzhe Yue, Ruihua Qi, Chuntao Li, and Hao Xu. 2023. Toward zero-shot character recognition: a gold standard dataset with radical-level annotations. In *Proceedings of the 31st ACM International Conference on Multimedia*. 6869–6877.
- [5] Xiaolei Diao, Daqian Shi, Hao Tang, Qiang Shen, Yanzeng Li, Lei Wu, and Hao Xu. 2022. RZCR: Zero-shot character recognition via radical-based reasoning. *arXiv preprint arXiv:2207.05842* (2022).
- [6] Jun Ding, Jiaoyan Wang, Alimjan Aysa, Xuebin Xu, and Kurban Ubul. 2024. Oracle bone inscriptions image retrieval based on metric learning. In *International Conference on Document Analysis and Recognition*. Springer, 159–173.
- [7] Sara Ghaboura, Ketan More, Ritesh Thawkar, Wafa Alghallabi, Omkar Thawakar, Fahad Shahbaz Khan, Hisham Cholakkal, Salman Khan, and Rao Muhammad Anwer. 2025. Time Travel: A Comprehensive Benchmark to Evaluate LMMs on Historical and Cultural Artifacts. *arXiv preprint arXiv:2502.14865* (2025).
- [8] Amirhosein Ghasemabadi, Muhammad Kamran Janjua, Mohammad Salameh, Chunhua Zhou, Fengyu Sun, and Di Niu. 2024. Cascadedgaze: Efficiency in global context extraction for image restoration. *arXiv preprint arXiv:2401.15235* (2024).
- [9] Ian Goodfellow, Jean Pouget-Abadie, Mehdi Mirza, Bing Xu, David Warde-Farley, Sherjil Ozair, Aaron Courville, and Yoshua Bengio. 2014. Generative adversarial nets. *Advances in neural information processing systems* 27 (2014).
- [10] Haisu Guan, Jimpeng Wan, Yuliang Liu, Pengjie Wang, Kaile Zhang, Zhebin Kuang, Xinyu Wang, Xiang Bai, and Lianwen Jin. 2024. An open dataset for the evolution of oracle bone characters: EVOBC. *arXiv preprint arXiv:2401.12467* (2024).
- [11] Haisu Guan, Huanxin Yang, Xinyu Wang, Shengwei Han, Yongge Liu, Lianwen Jin, Xiang Bai, and Yuliang Liu. 2024. Deciphering Oracle Bone Language with Diffusion Models. *arXiv preprint arXiv:2406.00684* (2024).
- [12] Jun Guo, Changhu Wang, Edgar Roman-Rangel, Hongyang Chao, and Yong Rui. 2015. Building hierarchical representations for oracle character and sketch recognition. *IEEE Transactions on Image Processing* 25, 1 (2015), 104–118.
- [13] Wenhui Han, Xinlin Ren, Hangyu Lin, Yanwei Fu, and Xiangyang Xue. 2020. Self-supervised learning of Orc-Bert augmentator for recognizing few-shot oracle characters. In *Proceedings of the Asian Conference on Computer Vision*.
- [14] Martin Heusel, Hubert Ramsauer, Thomas Unterthiner, Bernhard Nessler, and Sepp Hochreiter. 2017. Gans trained by a two time-scale update rule converge to a local nash equilibrium. *Advances in neural information processing systems* 30 (2017).
- [15] Jonathan Ho, Ajay Jain, and Pieter Abbeel. 2020. Denoising diffusion probabilistic models. *Advances in neural information processing systems* 33 (2020), 6840–6851.
- [16] Alain Hore and Djemel Ziou. 2010. Image quality metrics: PSNR vs. SSIM. In *2010 20th international conference on pattern recognition*. IEEE, 2366–2369.
- [17] Zhikai Hu, Yiu-ming Cheung, Yonggang Zhang, Peiyang Zhang, and Pui-ling Tang. 2024. Component-level oracle bone inscription retrieval. In *Proceedings of the 2024 International Conference on Multimedia Retrieval*. 647–656.
- [18] Hongxiang Huang, Daihui Yang, Gang Dai, Zhen Han, Yuyi Wang, Kin-Man Lam, Fan Yang, Shuangping Huang, Yongge Liu, and Mengchao He. 2022. Agtgan: Unpaired image translation for photographic ancient character generation. In *Proceedings of the 30th ACM international conference on multimedia*. 5456–5467.
- [19] Shuangping Huang, Haobin Wang, Yongge Liu, Xiaosong Shi, and Lianwen Jin. 2019. OBC306: A large-scale oracle bone character recognition dataset. In *2019 International Conference on Document Analysis and Recognition (ICDAR)*. IEEE, 681–688.
- [20] Hanqi Jiang, Yi Pan, Junhao Chen, Zhengliang Liu, Yifan Zhou, Peng Shu, Yiwei Li, Huaqin Zhao, Stephen Mihm, Lewis C Howe, et al. 2024. Oraclesage: Towards unified visual-linguistic understanding of oracle bone scripts through cross-modal knowledge fusion. *arXiv preprint arXiv:2411.17837* (2024).
- [21] Runhua Jiang, Yongge Liu, Boyuan Zhang, Xu Chen, Deng Li, and Yahong Han. 2023. OraclePoints: A Hybrid Neural Representation for Oracle Character. In *Proceedings of the 31st ACM International Conference on Multimedia*. 7901–7911.
- [22] Bang Li, Qianwen Dai, Feng Gao, Weiye Zhu, Qiang Li, and Yongge Liu. 2020. HWOBCC—a handwriting oracle bone character recognition database. In *Journal of Physics: Conference Series*, Vol. 1651. IOP Publishing, 012050.
- [23] Jing Li, Xueke Chi, QiuFeng Wang, Dahan Wang, Kaizhu Huang, Yongge Liu, and Cheng-lin Liu. 2024. A comprehensive survey of oracle character recognition: challenges, benchmarks, and beyond. *arXiv preprint arXiv:2411.11354* (2024).
- [24] Jing Li, Qiu-Feng Wang, Kaizhu Huang, Xi Yang, Rui Zhang, and John Y Goulermas. 2023. Towards better long-tailed oracle character recognition with adversarial data augmentation. *Pattern Recognition* 140 (2023), 109534.
- [25] Jing Li, Qiu-Feng Wang, Rui Zhang, and Kaizhu Huang. 2021. Mix-Up Augmentation for Oracle Character Recognition with Imbalanced Data Distribution. In *International Conference on Document Analysis and Recognition*. Springer, 237–251.
- [26] Jing Li, Qiu-Feng Wang, Rui Zhang, and Kaizhu Huang. 2021. Mix-Up Augmentation for Oracle Character Recognition with Imbalanced Data Distribution. In *Document Analysis and Recognition – ICDAR 2021*, Josep Lladós, Daniel Lopresti, and Seichi Uchida (Eds.). Springer International Publishing, Cham, 237–251.
- [27] Guoying Liu and Yangguang Wang. 2020. Oracle character image retrieval by combining deep neural networks and clustering technology. *IAENG International Journal of Computer Science* 47, 2 (2020), 08.
- [28] Yang Liu, Zhenyue Qin, Saeed Anwar, Pan Ji, Dongwoo Kim, Sabrina Caldwell, and Tom Gedeon. 2021. Invertible denoising network: A light solution for real noise removal. In *Proceedings of the IEEE/CVF conference on computer vision and pattern recognition*. 13365–13374.
- [29] Lin Meng. 2017. Recognition of Oracle Bone Inscriptions by Extracting Line Features on Image Processing. In *ICPRAM*. 606–611.
- [30] Alec Radford, Jong Wook Kim, Chris Hallacy, Aditya Ramesh, Gabriel Goh, Sandhini Agarwal, Girish Sastry, Amanda Askell, Pamela Mishkin, Jack Clark, et al. 2021. Learning transferable visual models from natural language supervision. In *International conference on machine learning*. PMLR, 8748–8763.
- [31] Robin Rombach, Andreas Blattmann, Dominik Lorenz, Patrick Esser, and Björn Ommer. 2022. High-resolution image synthesis with latent diffusion models. In *Proceedings of the IEEE/CVF conference on computer vision and pattern recognition*. 10684–10695.
- [32] Daqian Shi, Xiaolei Diao, Lida Shi, Hao Tang, Yang Chi, Chuntao Li, and Hao Xu. 2022. Charformer: A glyph fusion based attentive framework for high-precision character image denoising. In *Proceedings of the 30th ACM international conference on multimedia*. 1147–1155.
- [33] Daqian Shi, Xiaolei Diao, Hao Tang, Xiaomin Li, Hao Xing, and Hao Xu. 2022. Rcrn: Real-world character image restoration network via skeleton extraction. In *Proceedings of the 30th ACM international conference on multimedia*. 1177–1185.
- [34] Yu-Fei Shih, Zheng-Lin Lin, and Shu-Kai Hsieh. 2025. Reasoning Over the Glyphs: Evaluation of LLM’s Decipherment of Rare Scripts. *arXiv preprint arXiv:2501.17785* (2025).
- [35] Mei Wang and Weihong Deng. 2024. A dataset of oracle characters for benchmarking machine learning algorithms. *Scientific Data* 11, 1 (2024), 87.
- [36] Mei Wang, Weihong Deng, and Cheng-Lin Liu. 2022. Unsupervised structure-texture separation network for oracle character recognition. *IEEE Transactions on Image Processing* 31 (2022), 3137–3150.
- [37] Mei Wang, Weihong Deng, and Sen Su. 2024. Oracle character recognition using unsupervised discriminative consistency network. *Pattern Recognition* 148 (2024), 110180.
- [38] Pengjie Wang, Kaile Zhang, Xinyu Wang, Shengwei Han, Yongge Liu, Jimpeng Wan, Haisu Guan, Zhebin Kuang, Lianwen Jin, Xiang Bai, et al. 2024. An open dataset for oracle bone script recognition and decipherment. *arXiv preprint arXiv:2401.15365* (2024).
- [39] Wei Wang, Ting Zhang, Yiwen Zhao, Xinjin Jin, Harold Mouchere, and Xinguo Yu. 2022. Improving Oracle Bone Characters Recognition via A CycleGAN-Based Data Augmentation Method. In *International Conference on Neural Information Processing*. Springer, 88–100.
- [40] Zhendong Wang, Xiaodong Cun, Jianmin Bao, Wengang Zhou, Jianzhuang Liu, and Houqiang Li. 2022. Uformer: A general u-shaped transformer for image restoration. In *Proceedings of the IEEE/CVF conference on computer vision and pattern recognition*. 17683–17693.
- [41] Xuebin Yue, Hengyi Li, Yoshiyuki Fujikawa, and Lin Meng. 2022. Dynamic dataset augmentation for deep learning-based oracle bone inscriptions recognition. *ACM Journal on Computing and Cultural Heritage* 15, 4 (2022), 1–20.
- [42] Syed Waqas Zamir, Aditya Arora, Salman Khan, Munawar Hayat, Fahad Shahbaz Khan, and Ming-Hsuan Yang. 2022. Restormer: Efficient transformer for high-resolution image restoration. In *Proceedings of the IEEE/CVF conference on computer vision and pattern recognition*. 5728–5739.
- [43] Chongsheng Zhang, Bin Wang, Ke Chen, Ruixing Zong, Bo-feng Mo, Yi Men, George Alpanidis, Shanxiong Chen, and Xiangliang Zhang. 2022. Data-driven oracle bone rejoining: A dataset and practical self-supervised learning scheme. In *Proceedings of the 28th ACM SIGKDD Conference on Knowledge Discovery and Data Mining*. 4482–4492.
- [44] Chongsheng Zhang, Ruixing Zong, Shuang Cao, Yi Men, and Bo-feng Mo. 2021. AI-powered oracle bone inscriptions recognition and fragments rejoining. In *Proceedings of the Twenty-Ninth International Conference on International Joint Conferences on Artificial Intelligence*. 5309–5311.
- [45] Kai Zhang, Wangmeng Zuo, Yunjin Chen, Deyu Meng, and Lei Zhang. 2017. Beyond a gaussian denoiser: Residual learning of deep cnn for image denoising. *IEEE transactions on image processing* 26, 7 (2017), 3142–3155.
- [46] Lvmin Zhang, Anyi Rao, and Maneesh Agrawala. 2023. Adding conditional control to text-to-image diffusion models. In *Proceedings of the IEEE/CVF International Conference on Computer Vision*. 3836–3847.

- [47] Richard Zhang, Phillip Isola, Alexei A Efros, Eli Shechtman, and Oliver Wang. 2018. The unreasonable effectiveness of deep features as a perceptual metric. In *Proceedings of the IEEE conference on computer vision and pattern recognition*. 586–595.
- [48] Yi Zhang, Dasong Li, Xiaoyu Shi, Dailan He, Kangning Song, Xiaogang Wang, Hongwei Qin, and Hongsheng Li. 2023. Kbnnet: Kernel basis network for image restoration. *arXiv preprint arXiv:2303.02881* (2023).
- [49] Xinyi Zhao, Siyuan Liu, Yikai Wang, and Yanwei Fu. 2022. FFD Augmentor: Towards Few-Shot Oracle Character Recognition from Scratch. In *Proceedings of the Asian Conference on Computer Vision*. 1622–1639.
- [50] Xin-Lun Zhou, Xing-Cheng Hua, and Feng Li. 1995. A method of Jia Gu Wen recognition based on a two-level classification. In *Proceedings of 3rd International Conference on Document Analysis and Recognition*, Vol. 2. IEEE, 833–836.
- [51] Jun-Yan Zhu, Taesung Park, Phillip Isola, and Alexei A Efros. 2017. Unpaired image-to-image translation using cycle-consistent adversarial networks. In *Proceedings of the IEEE international conference on computer vision*. 2223–2232.

## A Ethical Discussions

The Oracle-P15K dataset is crucial for cultural preservation and academic research in the OBI research community. It can contribute to various OBI information processing tasks including, but not limited to, OBI generation and denoising. OBI generation not only facilitates the conservation and study of this invaluable cultural heritage but also enriches academic research with comprehensive material resources. Meanwhile, OBI denoising removes noise to enhance clarity for accurate interpretation and analysis. The integration of these two approaches establishes an innovative paradigm for artificial intelligence applications in cultural heritage restoration, thereby bridging the convergence of traditional civilization and modern technological innovation.

Besides, our dataset might also hold negative social impacts. Firstly, the use of unauthorized or unverified data in the generation process may raise ethical concerns regarding intellectual property rights and ownership claims over cultural heritage. Secondly, over-reliance on algorithmic restoration risks historical misinterpretation or fabrication, potentially undermining academic rigor. Additionally, misusing the technology for artifact forgery or commercial exploitation could compromise cultural authenticity and public trust. Therefore, ethical frameworks must prioritize legal data sourcing, transparent restoration protocols, and respect for the integrity of cultural heritage and the rights of its custodians.

## B Operational Details

Firstly, we import the style image by clicking the import button in the main interface of Procreate. The pop-up displays the directory of the style images, where we select the target image. Subsequently, we click the settings button to show the information of different layers. We need to add a new layer so that the drafts we write can be saved separately. Then, we swipe the attribute bar of the original layer to the left and lock it by clicking the lock button on the right. After that, the glyph is meticulously traced over the style image. Once the writing process is complete, the original layer is hidden, and the newly added layer is saved as the final glyph image.

## C Implementation Details

### C.1 Implementation Details of OBIDiff

The proposed OBIDiff is trained on an NVIDIA RTX 4090 GPU for 200 epochs using the AdamW optimizer with a weight decay of 0.01,  $\beta_1 = 0.9$ , and  $\beta_2 = 0.99$ . During training, the learning rate is set to  $1e-5$ . We use a batch size of 1, and the size of each image is set to  $128 \times 128$ . The entire training process spans over 2 days.

### C.2 Implementation Details of Classifier

Our custom-built classifier is built upon ResNet-50. The model is implemented using the PyTorch platform and trained on an NVIDIA RTX 4090 GPU for 500 epochs with the Adam optimizer. The learning rate is set to  $5e-5$  and the weight decay is set to 0.01. We use a batch size of 512, and the size of each image is set to  $128 \times 128$ . Random rotation and horizontal flipping techniques are used for data augmentation.

## D Visualizations

We conduct feature map visualizations using *matplotlib* to analyze the hierarchical feature extraction patterns in convolutional neural networks. As shown in Fig. 12, we systematically compare the activation patterns of both the initial and final convolutional layers within each residual stage of ResNet-50. Through comparative visualizations of feature maps generated by separately trained models on handprint and rubbing OBI datasets, we have two key observations. First, shallow-layer features (e.g., conv1 and final conv layer of stage 1) exhibit *striking structural similarities* between different models, particularly in edge detection and basic texture response patterns. Second, deeper layers (final conv layers of stage 3-4) demonstrate *divergent specialization*. The handprints-trained model develops enhanced sensitivity to stroke endings and bifurcations, while the rubbings-trained model prioritizes texture continuity. This progressive divergence suggests that while early convolutional layers learn domain-agnostic visual primitives, deeper layers evolve task-specific representations through residual learning. Therefore, the disparity in handprint and rubbing OBI images has a substantial impact on OBI recognition.

## E Details of the User Preference Study

We utilize HTML, CSS, and JavaScript to develop a human evaluation user interface for OBI. As shown in Fig. 13, the interface presents either a ground truth image or a pseudo image generated by our OBIDiff in each round. Participants can click the button below to determine whether the current image is a real-world OBI rubbing image or a generated image. The navigation within the evaluation workflow is facilitated by *Previous* and *Next* buttons. Once the evaluation is complete, the user can click the *Export* button to generate a brief evaluation report. This report includes relevant user information and an assessment of the user's performance in the evaluation. We present the detailed results of the user preference study in Table 5.

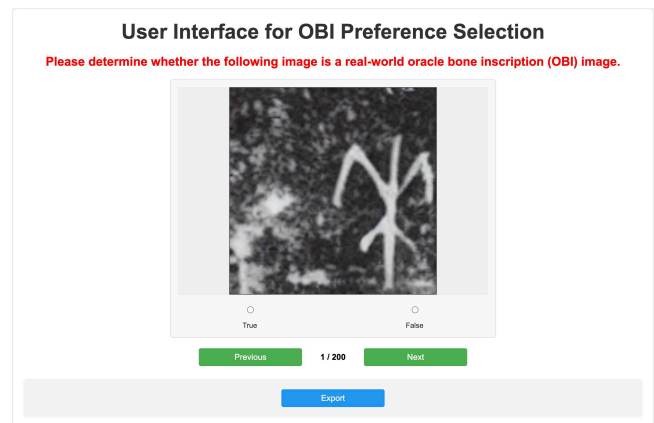


Figure 13: User interface of human evaluation in OBI preference selection task.

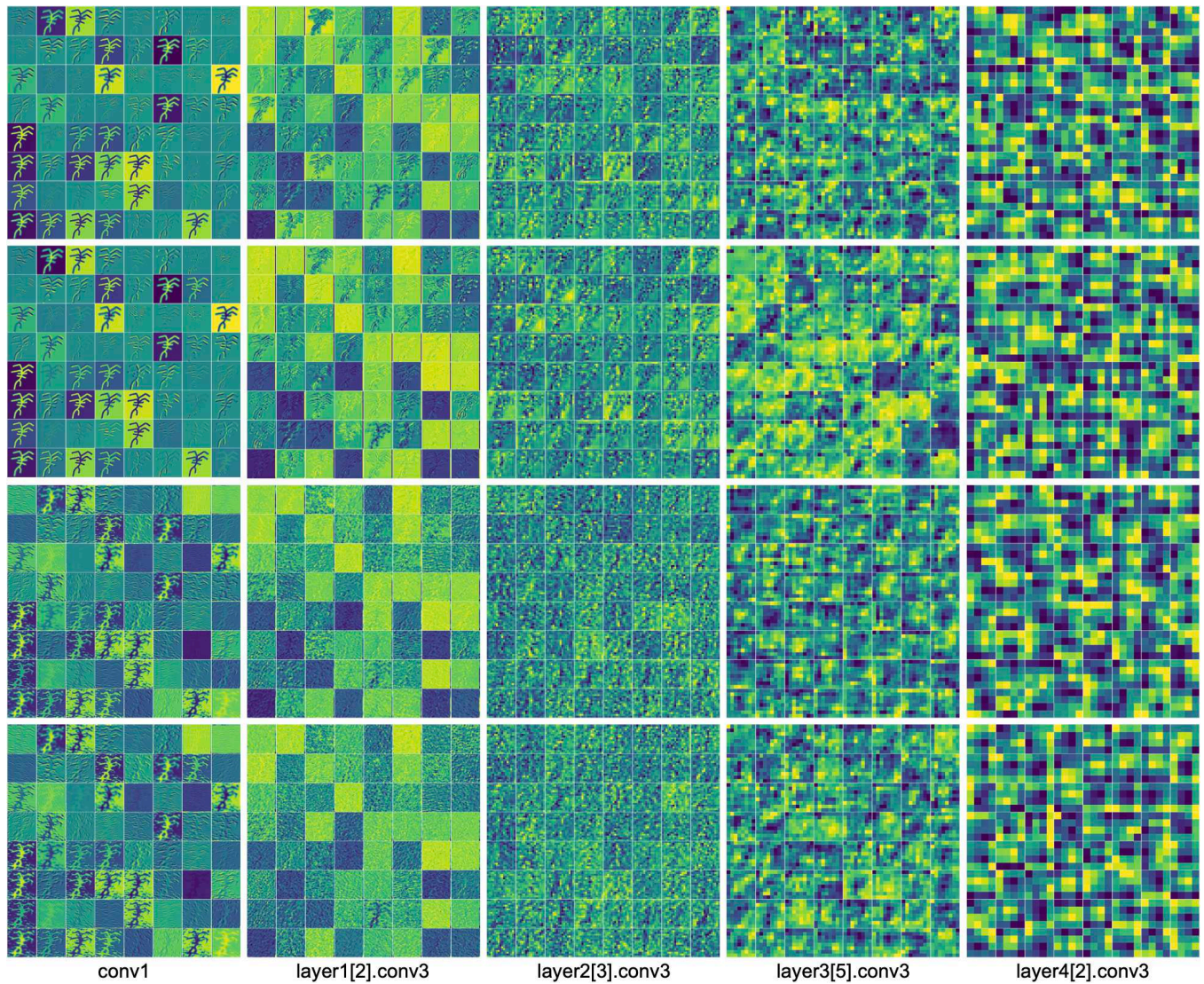


Figure 12: Feature map visualizations of ResNet-50. From top to bottom we present the visualizations of feature maps extracted from the handprint and rubbing images by the models trained on handprint and rubbing OBI datasets, respectively. For each image, we visualize the feature map of each channel.

Table 5: Detailed results of the user study.

|               | 1    | 2    | 3    | 4    | 5    | 6    | 7    | 8    | 9    | 10   | 11   | 12   | 13   | 14   | 15   | Average |
|---------------|------|------|------|------|------|------|------|------|------|------|------|------|------|------|------|---------|
| Precision (%) | 0.56 | 0.55 | 0.50 | 0.53 | 0.49 | 0.48 | 0.52 | 0.54 | 0.58 | 0.47 | 0.54 | 0.58 | 0.54 | 0.44 | 0.49 | 0.52    |
| Recall (%)    | 0.53 | 0.86 | 0.88 | 0.44 | 0.62 | 0.56 | 0.40 | 0.56 | 0.48 | 0.16 | 0.63 | 0.68 | 0.63 | 0.47 | 0.66 | 0.57    |
| F1 Score      | 0.54 | 0.67 | 0.64 | 0.48 | 0.55 | 0.52 | 0.45 | 0.55 | 0.53 | 0.24 | 0.58 | 0.63 | 0.58 | 0.46 | 0.56 | 0.53    |
| Duration (s)  | 1126 | 2501 | 3207 | 1568 | 946  | 823  | 1015 | 867  | 1952 | 483  | 485  | 497  | 595  | 3155 | 2256 | 1432    |



Figure 14: More generation results from our OBIDiff and other OBI generation methods.

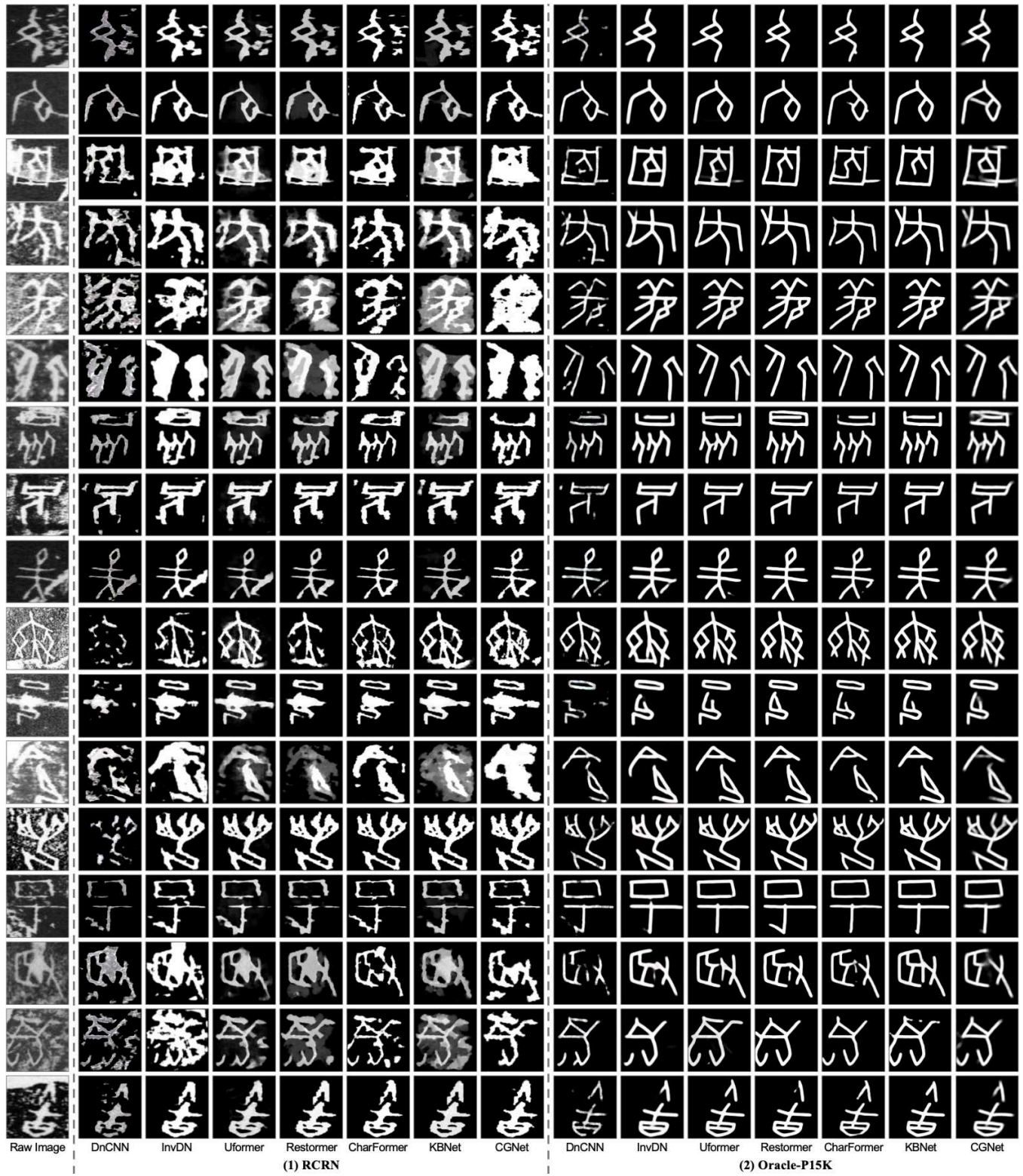


Figure 15: More denoising results from generic and OBI denoising baselines.